Multi-physics simulation for predicting the permeability change of single rock fracture due to geochemical effect depending on pH condition

Sho Ogata[i], Hideaki Yasuhara[ii], Naoki Kinoshita[ii], Takeru Kumagai[ii], Toru Inui[i],
Seiki Mishima [i] and Kiyoshi Kishida[iii]

i) Division of Global Architecture, Osaka University, 2-1 Yamadaoka, Suita, Osaka 565-0871, JAPAN.
ii) Department of Civil and Environmental Engineering, Ehime University, 3 Bunkyocho, Matsuyama 790-8577, JAPAN.
iii) Department of Urban Management, Kyoto University, Nishikyo-ku, Kyotodaigaku Katsura, Kyoto 615-8540, JAPAN.

ABSTRACT

A multi-physics simulator, with geochemical reactions that depend on the pH condition, was proposed. The simulator was validated by replicating the measurements of the evolving permeability and the solute concentrations in a single rock fracture obtained from flow-through experiments under different pH conditions. Then, the changes in fracture permeability during the virtual long-term flow-through tests were predicted by assuming the permeant under various pH, stress, and temperature conditions. The predicted results show that the rate of permeability reduction under a pH of 11 was about 10 times faster than that under a pH of 7.0, and the impact of the pH condition was confirmed.

Keywords: permeability, single rock fractures, geochemical reactions, pH condition

1 INTRODUCTION

When investigating the performance of a rock mass, which works as a natural barrier for a geological repository of high-level radioactive waste (HLW), it is essential to predict the long-term permeability change in the rock fractures that defines the groundwater flow. From previous experimental works (e.g., Yasuhara et al., 2011), it is well known that the permeability of rock fractures is altered by the geochemical reactions enhanced by stress and temperature, such as the mineral dissolution/precipitation within the rock fractures over a long duration. In particular, pressure dissolution, which is mineral dissolution at the asperity contacts within fractures, exerts a significant impact on the evolution of fracture permeability (e.g., Yasuhara et al., 2011). In addition, the above-mentioned geochemical reactions also depend on the chemical condition of the fluid, such as the pH condition (e.g., Kinoshita and Yasuhara, 2012; Yasuhara et al., 2012). Thus, they may be affected by the inflow of the alkaline cement solution from an artificial barrier, which can be assumed in the actual environment where HLW is disposed. However, numerical simulators that can consider the influence of the pH condition of the fluid on the permeability change of rock fractures due to geochemical effects, have not yet been well developed or validated by comparisons with experimental data.

For example, Ogata et al. (2018) proposed a coupled thermo-hydro-mechanical-chemical (THMC) simulator based on FEM, which can reproduce the permeability evolution due to the geochemical effects obtained from flow-through experiments by employing single fractures of granite and mudstone (Yasuhara et al., 2011). However, this simulator does not consider the influence of the pH on the geochemical reactions. Although Bond et al. (2016) presented a coupled THMC simulator that considers the pH dependence on geochemical reactions, it was applied only to the simulation of flow-through experiments using deionized water (pH~7) as permeable water (Yasuhara et al., 2011). Yasuhara et al. (2012) attempted to replicate the change in effluent solute concentrations with time measured from a series of flow-through experiments on a single rock fracture in granite under various pH conditions (Kinoshita and Yasuhara, 2012) by using a simple rate law for kinetic mineral dissolution. However, their work did not take into account the influence of the pressure dissolution.

In this study, a coupled THMC simulator was proposed by adding the pH dependence on the geochemical reactions, such as pressure dissolution, into our previous simulator (Ogata et al., 2018). Subsequently, the simulator was applied to replicate the results measured from flow-through experiments on single rock fractures in granite under various pH conditions, namely, permeable water, stressed, and temperature-elevated conditions (Kinoshita and Yasuhara, 2012), and validated by comparisons with experimental data. Finally, the differences in the long-term permeability change of rock fractures under various pH conditions were examined by the simulator.

2 SIMULATOR DESCRIPTION

The simulator used in this work is based on FEM that

https://doi.org/10.3208/jgssp.v09.cpeg045

can calculate the THMC coupling process including mineral dissolution at the asperity contacts and the pore wall within rock fractures that depend on the pH condition. This simulator was presented by incorporating the geochemical reactions depending on the pH value into our previous simulator (Ogata et al., 2018). In the target experiments for the numerical simulation of this work, the temperature and stress distributions within rock specimens can be assumed homogeneous. Thus, in this work, only the coupled process, including the fluid flow, reactive transport with geochemical effects, and updating the geometry with time within rock fractures, are solved by the FEM engine of COMSOL MULTIPHYSICS.

The fluid flow behavior in the fractures of saturated rock is predicted by the conservation of water mass and by assuming the Darcian flow, as follows:

$$\frac{\partial(\rho_w \varphi)}{\partial t} + \nabla \cdot (\rho_w \boldsymbol{u}) = f_w \tag{1}$$

$$\boldsymbol{u} = -\frac{k}{\mu} \nabla p \tag{2}$$

$$k = \frac{b_h^{\,2}}{12} \tag{3}$$

where ρ_w [kg m^{-3}] is the density of the fluid, φ [-] is the porosity, $\boldsymbol{u}$ [m s^{-1}] is the fluid velocity vector, f_w [kg m^{-3} s^{-1}] is the source term for the flow, k [m^2] is the rock permeability, μ [Pa s] is the fluid dynamic viscosity, p [Pa] is the water pressure, and b_h [m] is the hydraulic aperture of the rock fracture.

The behavior of the reactive transport in rock fractures is described by solving the basic advection-diffusion equation. The mechanical dispersion and sorption processes are not considered here.

$$\frac{\partial (c_i \varphi)}{\partial t} + \boldsymbol{u} \cdot \nabla c_i = \nabla \cdot (\tau \varphi D_{b,i} \nabla c_i) + r_i \tag{4}$$

where c_i [mol m^{-3}] is the concentration of solute i in the pore water, $D_{b,i}$ [m^2 s^{-1}] is the diffusion coefficient tensor, τ [-] (τ=1.0) is the coefficient related to tortuosity, and r_i [mol m^{-3} s^{-1}] is the source term of solute i. In this work, the target rock consists of multi-minerals. When the number of minerals included in the targeted rocks is m, the total solute source is expressed by

$$r_i = \sum_j^m v_i R_j \tag{5}$$

where v_i [-] is the stoichiometry coefficient of solute i in the pore water and R_j [mol m^{-3} s^{-1}] is the rate of the geochemical reactions for mineral j.

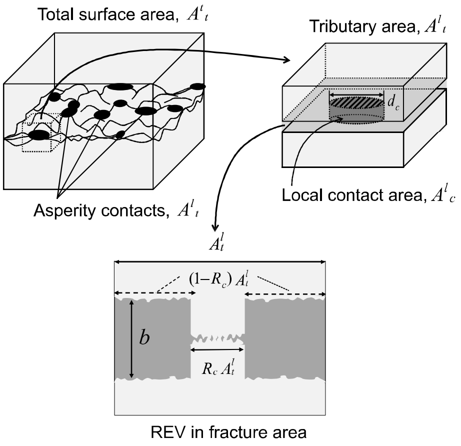
Total surface area, $A^t{}_t$
Tribulary area, $A^l{}_t$
d_c
Asperity contacts, $A^l{}_t$
Local contact area, $A^l{}_c$
A^l_t
$(1-R_c)\,A^l_t$
b
$R_c\,A^l_t$
REV in fracture area

Fig. 1. Geometrical model that includes representative element within rock fracture domain (Yasuhara et al., 2011). Tributary area $A^l{}_t$ is the representative element composed of asperity contact area $R_c\,A^l{}_t$ and pore space.

The kinetic mineral dissolution/precipitation at the free surface of the rock fractures (i.e., free-face dissolution/precipitation) and the pressure dissolution at the asperity contact of the rock fractures are considered as geochemical reactions in the simulator. Therefore, R_j is represented by

$$R_j = R_j^{FF} + R_j^{PS} \tag{6}$$

where R_j^{FF} [mol m^{-3} s^{-1}] and R_j^{PS} [mol m^{-3} s^{-1}] are the rates of free-face dissolution/precipitation and pressure dissolution of mineral j on the rock fracture, respectively. When the micro fracture area that is composed of contacting asperities and pore space is set as the representative element shown in Fig. 1, the rate of the free-face dissolution/precipitation of mineral j, R_j^{FF}, can be expressed by (Ogata et al., 2018)

$$R_j^{FF} = 2\chi_j f_{r,j} k_{+,j} \left(1 - \frac{Q_j}{K_{eq,j}}\right) / b \tag{7}$$

where $f_{r,j}$ [-] is the roughness factor of mineral j, χ_j [-] is the volumetric ratio of mineral j, $k_{+,j}$ [mol m^{-2} s^{-1}] is the mineral dissolution rate constant, Q_j [-] is the ionic activity product of mineral j, $K_{eq,j}$ [-] is the equilibrium constant of mineral j, and b [m] is the mechanical aperture of the rock fracture. In this work, Eq. (7) is reformulated to a form which does not consider the effect of precipitation by assuming the system of interest under the far-from-equilibrium condition, namely,

$$R_j^{FF} = 2\chi_j f_{r,j} k_{+,j} / b \tag{8}$$

The rate of pressure dissolution at the contacting asperities within the fracture, R_j^{PS}, is expressed as (Ogata et al., 2018)

$$R_j^{PS} = \frac{3 f_{r,j} \chi_j V_{m,j} k_{+,j} R_c}{RTb(1 - R_c)} \left(\frac{\sigma_n}{R_c} - \sigma_c\right) \tag{9}$$

where $V_{m,j}$ [m^3 mol^{-1}] is the molar volume of the solid of mineral j, R [kJ mol^{-1} K^{-1}] is the gas constant, R_c [-] is the contact area ratio of the fracture asperities, σ_n [MPa] is the compressive stress acting on the rock domain, and σ_c [Pa] is the critical stress.

The mineral dissolution rate constants, that are significantly important parameters for calculating geochemical reactions, are represented by the Arrhenius expression with dependence on the temperature and the pH condition, given as (Palandri and Kharaka, 2004)

$$k_{+,j} = k_{1,j} a_{H^+}^{n1} + k_{2,j} + k_{3,j} a_{H^+}^{n3} \tag{10}$$

$$k_{i,j} = k_{i,j}^{298.15K} \exp\left[\frac{-E_{i,j}}{R}\left(\frac{1}{T} - \frac{1}{298.15K}\right)\right] \tag{11}$$

where $k_{i,j}^{298.15K}$ $(i = 1, 2, 3)$ [mol m^{-2} s^{-1}] is the rate constant of mineral j at 298.15K (25°C) and pH = 0 under acid, neutral, and base mechanisms, respectively, $E_{i,j}$ $(i = 1, 2, 3)$ [J mol^{-1}] is the activation energy of mineral j under acid, neutral, and base mechanisms, respectively, a_{H+} is the activity of H$^+$, and n_1 and n_3 are the dimensionless catalysis constants for the acid and base mechanisms, respectively.

In this work, the fracture aperture is induced only by the geochemical reactions of both the free-face dissolution and the pressure dissolution. The fracture aperture at an arbitrary time is given as follows:

$$b(t) = b_0 + \int \dot{b}^{FF}(t)dt + \int \dot{b}^{PS} dt \tag{12}$$

where b_0 [m] is the initial fracture aperture, $\dot{b}^{FF}$ [m s^{-1}] is the rate of fracture aperture change by the free-face dissolution, and $\dot{b}^{PS}$ [m s^{-1}] is the rate of fracture aperture change by the pressure dissolution. The rates of aperture change by free-face dissolution and pressure dissolution in the rock fracture are defined as follows:

$$\dot{b}^{FF} = \sum_j^n 2 f_{r,j} \chi_j (1 - R_c) V_{m,j} k_{+,j} \tag{13}$$

$$\dot{b}^{PS} = \sum_j^n \frac{3 f_{r,j} \chi_j k_{+,j} V_{m,j}^2}{RT}\left(\frac{\sigma_n}{R_c} - \sigma_c\right) \tag{14}$$

The contact area of the fracture is altered depending on the change in fracture aperture. This relationship between the fracture aperture and the contact area of the fracture may be given by the following simple function (Yasuhara et al., 2011):

$$b = b_r + (b_0 - b_r)\exp(-(R_c - R_{c0})/a), \tag{15}$$

where b_r [m] is the residual fracture aperture and a [-] is a constant. The hydraulic aperture of a rock fracture is calculated by using the mechanical aperture and the contact area ratio of the fracture asperities (Walsh, 1981).

$$b_h^3 = \frac{(1 - R_c)}{(1 + R_c)} b^3 \tag{16}$$

3 VALIDATION OF SIMULATOR

3.1 Simulating experimental results

In order to validate the proposed simulator, the simulator is applied to replicate the experimental results. The target experiments for the numerical simulation are the flow-through experiments performed by employing the granite specimens (Kinoshita and Yasuhara, 2012). As shown in Fig. 2, the rock specimen utilized for the experiment includes an artificial single fracture. The experimental system is also depicted in Fig. 2. Two experiments, namely, E-4 and E-7, are conducted using cylindrical specimens of granite (E-4: 29.8 mm in diameter × 57.4 mm in length, E7: 29.7 mm in diameter × 62.1 mm in length). The experimental conditions of E-4 and E-7 are denoted in Table 1. E-4 is performed using deionized water (pH~7) as the permeant at a confining pressure of 5 MPa, temperatures of 25-90°C, and differential water pressure of 0.1-0.13 MPa. E-7 is conducted using a NaOH aqueous solution (pH ~ 11) as the permeant at a confining pressure of 5.0 MPa, temperatures of 25-90°C, and differential water pressure of 0.015-0.05 MPa. In the two experiments, equivalent hydraulic aperture $<b_h>$ is calculated from the measured flow rate via the parallel plate approximation, namely,

$$<b_h> = \left(\frac{12\mu l Q}{w \Delta p}\right)^{1/3} \tag{17}$$

where Q [m^3 s^{-1}] represents the measured flow rates, Δp [Pa] is the differential water pressure, w [m] is the width of the specimen, and l [m] is the length of the specimen. The equivalent permeability is derived based on an equivalent hydraulic aperture.

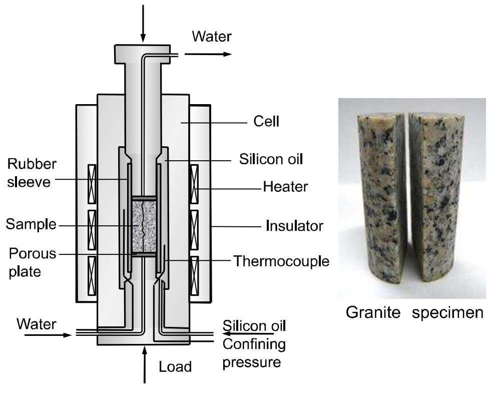

Fig. 2. Schematics of flow-through experiment (left side) from Yasuhara et al. (2011) and rock specimen (right side).

Table 1. Experimental conditions.

Specimen	E-4	E-7
Confining pressure [MPa]	5.0	5.0
System temperature [°C]	25-90	25-90
pH of permeant	7.0	11.0

$$< k >= \frac{<b_h>^2}{12} \tag{18}$$

The fluid samples were taken from the flow outlet in the two experiments in order to measure the pH and determine the effluent Si, Al, K, Fe, Ca, Na, and Mg aqueous concentrations, using inductively coupled plasma atomic emission spectrometry (ICP-AES).

3.2 Setup of numerical simulations

The experimental measurements of the evolution in the equivalent permeability of the rock fracture and the effluent element concentrations for E-4 and E-7, are replicated by the simulator proposed in this work. The calculation domains that express the rock fracture area of the specimens in 2D are set to be square with the length and width corresponding to those of the specimens used in the experiments (Fig. 3). In the simulations for E-4 and E-7, the initial hydraulic aperture and the contact area ratio of the fracture are assumed homogeneous within the entire domains. The values for the initial hydraulic aperture are determined from the experimental data for E-4 and E-7. The values for the initial contact area ratio, the residual aperture, and constant *a* were not measured in the target experiments. Therefore, these parameters are set to be the values assumed by Yasuhara et al. (2011). In the simulation for E-4, all the element (Si, Al, K, Fe, Ca, Na, and Mg) concentrations of 0 mol m^{-3} are prescribed as the fixed concentration condition of the inlet boundary, while only the Na concentration at the inlet boundary is set to be the non-zero value of 1.0 mol m^{-3} corresponding to the inflow of the NaOH aqueous solution for E-7. The isothermal condition within the entire domains changes from 25°C to 90°C, corresponding to the experimental period in the experiments. Differential pressures of 0.1-0.13 MPa and 0.015-0.05 MPa are set at the inlet and outlet boundaries of the geometry for E-4 and E-7, respectively. The calculation domains for E-4 and E-7 are assumed to be composed of five minerals, namely, quartz (50 vol%), orthoclase (12 vol%), albite (10 vol%), anorthite (20 vol%), and biotite (8.0 vol%), after referring to the literature (Yasuhara et al., 2011). The roughness factor of the quartz, orthoclase, albite, and anorthite is 7.12 (Yasuhara et al., 2011), while that of biotite is 512 (Kalinowski and Schweda, 1996). The important parameters of the kinetic dissolution rate constant (see Eqs. (10) and (11)) for the minerals considered in the simulations obtained from Palandri and Kharaka (2004) are given in Table 2. Each setup of the parameters used in the simulations is summarized in Table 3. In the simulations, the equivalent hydraulic aperture is calculated by the following equation:

$$<b_h>= \left(\frac{12 \mu l \Sigma q}{w \Delta p} \right)^{1/3} \tag{19}$$

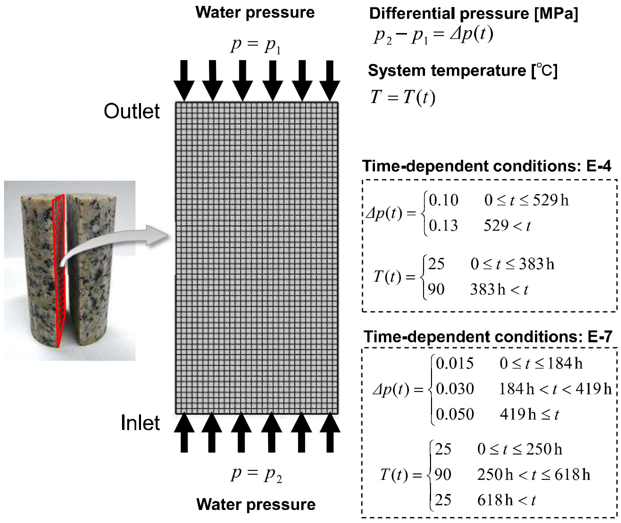
Water pressure
$p = p_1$
Differential pressure [MPa]
$p_2 - p_1 = \Delta p(t)$
System temperature [℃]
$T = T(t)$
Outlet
Time-dependent conditions: E-4
$\Delta p(t) = \begin{cases} 0.10 & 0 \le t \le 529\,\mathrm{h} \\ 0.13 & 529 < t \end{cases}$
$T(t) = \begin{cases} 25 & 0 \le t \le 383\,\mathrm{h} \\ 90 & 383\,\mathrm{h} < t \end{cases}$
Time-dependent conditions: E-7
$\Delta p(t) = \begin{cases} 0.015 & 0 \le t \le 184\,\mathrm{h} \\ 0.030 & 184\,\mathrm{h} < t < 419\,\mathrm{h} \\ 0.050 & 419\,\mathrm{h} \le t \end{cases}$
$T(t) = \begin{cases} 25 & 0 \le t \le 250\,\mathrm{h} \\ 90 & 250\,\mathrm{h} < t \le 618\,\mathrm{h} \\ 25 & 618\,\mathrm{h} < t \end{cases}$
Inlet
$p = p_2$
Water pressure

Fig. 3. Model geometry discretized by finite element and boundary conditions for simulations of E-4 and E-7.

Table 2. Parameters of kinetic dissolution rate constant for minerals obtained from Palandri and Kharaka (2004).

Parameter	Quartz	Ortho clase	Anor thite	Albite	Biotite
$\log k_1^{298.15K}$	-	-10.66	-3.50	-10.16	-9.84
$\log k_2^{298.15K}$	-13.99	-12.56	-9.12	-12.56	-12.55
$\log k_3^{298.15K}$	-	-21.2	-	-15.6	-
E_1 [kJ/mol]	–	51.7	16.6	65	22.0
E_2 [kJ/mol]	87.6	38.0	17.8	69.8	22.0
E_3 [kJ/mol]	-	94.1	1.411	71.0	-
n_1	-	0.50	-	0.457	0.525
n_3	-	-0.823	-	-0.572	-

Table 3. Parameters used in the simulations of E-4 and E-7 (Yasuhara et al., 2011).

Parameter	Value
Critical stress σ_c [MPa]	100
Residual aperture b_r [μm]	0.40
Initial contact area ratio R_{c0} [-]	0.01
Constant *a*	0.02

where Σq is the total flux flowing through the numerical domain, Δp [Pa] is determined by the differential water pressure between the inlet and outlet boundaries of the numerical domain. The effluent element concentrations are obtained at the outlet boundary of the analysis domain.

3.3 Comparisons with experimental results

Predictions of the permeability change with time, together with experimental measurements for E-4 and E-7, are shown in Fig. 4. The figure shows that the predictions well capture the trends of the decrease in permeability measured in experiments for E-4 and E-7. In the case of E-4, the predicted permeability is similar to the measurements throughout the experimental period and shows an excellent agreement with the actual data until the end of the experiments. From comparisons of the experimental results between E-4 and E-7, it is implied that the amount of permeability reduction enhanced by the increasing temperature of E-7 is greater than that of E-4. The simulator replicates this phenomenon well. In the case of E-7, the predicted permeability slightly underestimates the measurements after the temperature is decreased from 90°C to 25°C. In this period, the actual permeability increases. As this behavior may be attributed to the release of thermal expansion due to temperature degradation, a simulator that does not consider the mechanical deformation of the fracture due to the thermal effect cannot describe this behavior.

The predicted changes in concentrations for the seven elements (Si, Al, K, Fe, Ca, Na, and Mg) for E-4 and E-7 are shown in Fig. 5, together with the corresponding experimental data. The predicted element concentrations for E-4, except for K and Na, agree relatively well with the experimental data, although generally underestimating the experimental measurements. The gaps related to the Na and K concentrations are unexplainable at this stage. In the case of E-7, the predicted concentrations for five elements (Si, Fe, Ca, Na, and Mg), but not for Al and K, can replicate the experimental data within about one order of gaps. The overestimation of the Al concentration may be caused by an unaccounted contribution of the precipitation at the free surface of the fractures. In the experiment for E-7, the concentration of Na remains high due to the continuous inflow of the NaOH aqueous solution. Due to the situation, the albite including element Na may reach the supersaturated state and the precipitation of albite may occur continuously, which should be further examined. Overall, it is shown that the current simulator can follow the evolution of the fracture permeability of rock and the reactive transport behavior within a rock fracture due to geochemical effects depending on the pH conditions.

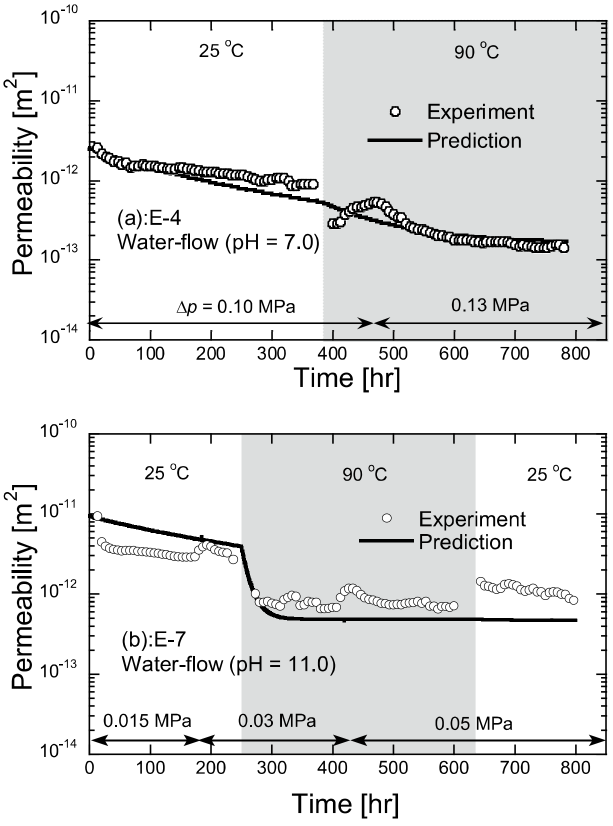

Fig. 4. Comparisons of fracture permeability evolution with time between measurements and predictions for (a) E-4 and (b) E-7.

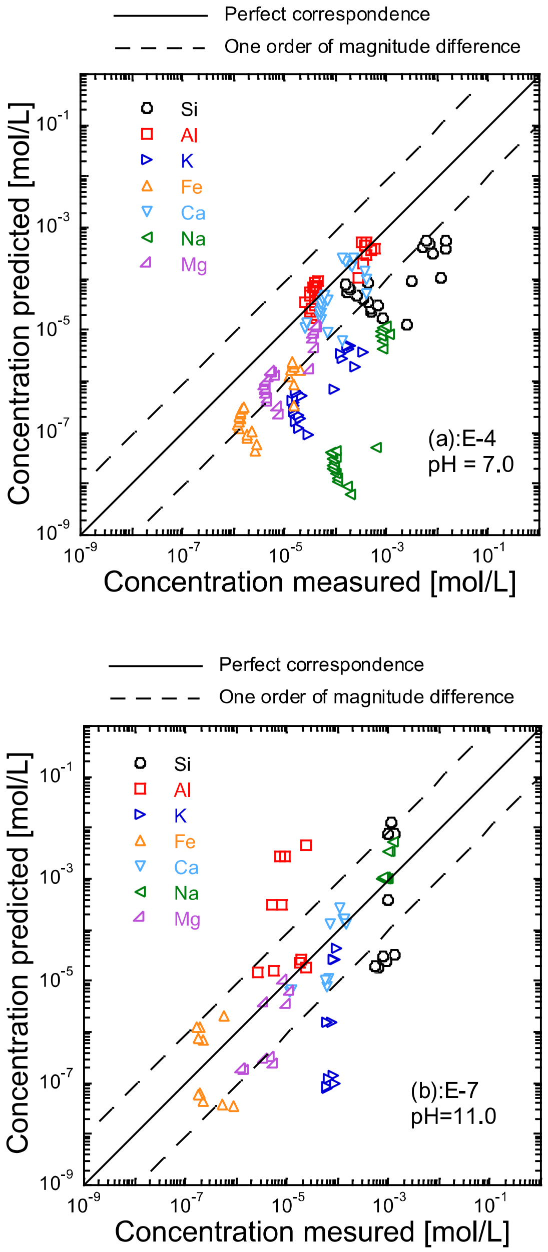

Fig. 5. Comparisons of element concentrations between measurements and predictions for (a) E-4 and (b) E-7.

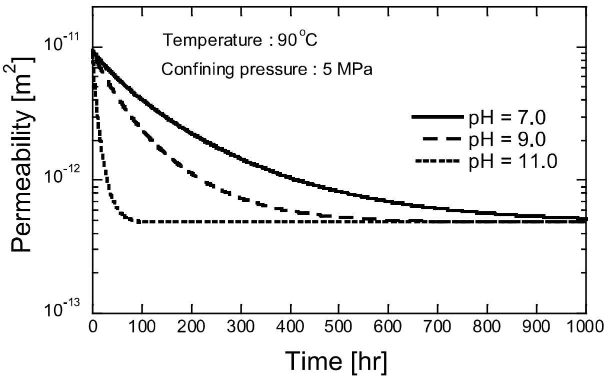

Fig. 6. Long-term prediction of fracture permeability under various pH conditions.

3.4 Long-term prediction of permeability evolution under various pH conditions

In order to quantitatively examine the difference in permeability evolution depending on the pH condition, long-term predictions under various pH conditions (pH = 7.0, 9.0, 11.0) were performed (Fig. 6). A constant temperature of 90 °C and a confining pressure of 5 MPa are applied to a numerical specimen that has the same dimensions as E-7. The differential water pressure is set to be 0.05 MPa. The figure shows that the rate of the permeability reduction increases with an increase in the pH value and that the time it takes to reach the residual value under a pH of 11 is about one tenth of that under a pH of 7.0. These results confirm the significant impact of the pH condition on the permeability evolution of a rock fracture with time under the coupled THMC condition.

4 CONCLUSIONS

A coupled THMC simulator, *IPSACC* (Interface for Pressure Solution Analysis under Coupled Conditions), was presented by employing the geochemical reactions depending on the pH condition. Subsequently, the simulator was utilized to replicate the changes in permeability and element concentrations within single rock fractures mainly due to the geochemical effects measured from two flow-through experiments in granite, that were conducted using permeants of different pH levels under stressed and temperature–elevated conditions. The simulated reductions in fracture permeability were in good agreement with the actual data of both experiments and exactly captured the observed difference in the reduction rate depending on the pH condition. The effluent element concentrations induced by the reactive transport obtained from the experiments were reproduced relatively well by the predictions. All comparisons between the experimental data and the predictions provide confidence for using the proposed simulator to estimate the alteration of permeability and reactive transport behavior within rock fractures resulting from the geochemical reactions depending on the pH condition. Finally, the long-term predictions of the fracture permeability under various pH conditions and constant thermal-mechanical loading were performed, and the significant increase in the rate of permeability decrease by the transition of the pH condition from neutral to alkaline was confirmed. The results obtained from this work suggest that considering and accurately modeling the impact of the pH condition on geochemical reactions will play an important role in understanding the property of the fluid flow within fractured rock under coupled THMC conditions in actual engineering problems, such as the geological disposal of HLW.

ACKNOWLEDGEMENTS

This work was supported by JSPS KAKENHI, subject nos. 18J12549 and 19H02237, and by research grants provided by the Kajima Foundation and the Casio Science Promotion Foundation, Japan.

REFERENCES

1) Bond, A., Brusky, I., Chittenden, N., Feng, X-T., Kolditz, O., Lang, P., Lu, R., McDermott, C., Neretnieks, I., Pan, P-Z., Sembera, J., Shao, H. and Yasuhara, H. (2016): Development of approaches for modelling coupled thermal–hydraulic–mechanical–chemical processes in single granite fracture experiments, *Environ. Earth. Sci*. 75: 1313.
2) Kalinowski, BE. and Schweda, P. (1996): Kinetics of muscovite, phlogopite and biotite dissolution and alternation at pH 1-4, room temperature, *Geochm. Cosmochim. Act*, 60, 367-385.
3) Kinoshita, N. and Yasuhara, H. (2012): Evolution of Fracture Permeability in Granite under High Temperature and High Confining Pressure Condition, *Journal of MMIJ*, 128, 72-78 (in Japanese).
4) Ogata, S., Yasuhara, H., Kinoshita, N., Cheon, DS. and Kishida, K. (2018): Modeling of coupled thermal-hydraulic-mechanical-chemical process for predicting the evolution in permeability and reactive transport behavior within single rock fractures, *Int. J. Rock Mech. Min. Sci*, 107, 271-281.
5) Palandri, JL. and Kharaka, YK. (2004): A compilation of rate parameters of mineral-water interaction kinetics for application to geochemical modelling, US Geological Survey open file report 2004–108, USA.
6) Yasuhara, H., Kinoshita, N., Ohfuji H., Lee DS., Nakashima, S. and Kishida, K. (2011): Temporal alteration of fracture permeability in granite under hydrothermal conditions and its interpretation by coupled chemo-mechanical model. *Appl Geochem*, 26, 2074–2088.
7) Yasuhara, H., Hashimoto, K. and Kinoshita, N. (2012): Evaluation of Dissolution Equation in Granite Examination by Flow-Through Dissolution Experiment under Temperature and pH conditions Controlled, *Journal of MMIJ*, 128, 79-85 (in Japanese).
8) Walsh, J. (1981): Effect of pore pressure and confining pressure on fracture permeability. *Int. J. Rock. Mech. Min Sci. Geomech*, 18(5), 429–435.